Fusion Engineering and Design 141 (2019) 25–29

Contents lists available at ScienceDirect

Fusion Engineering and Design

journal homepage: www.elsevier.com/locate/fusengdes

Simultaneous detection of neoclassical tearing mode and electron cyclotron current drive locations using electron cyclotron emission in DIII-D

A.O. Nelson[a], R.J. La Haye[b], M.E. Austin[c], A.S. Welander[b], E. Kolemen[d,*]

[a] Princeton Plasma Physics Laboratory, PO Box 45, Princeton, NJ 08543-0451, USA
[b] General Atomics, P.O. Box 85608, San Diego, CA 92186-5608, USA
[c] University of Texas, Austin, TX 78712, USA
[d] Princeton University, Princeton, NJ 08544, USA

ARTICLE INFO

Keywords:
NTM
Tokamak control
ECCD
ECE
DIII-D
Plasma

ABSTRACT

Accurate real-time measurements of magnetic island and electron cyclotron current drive (ECCD) locations are essential for efficient suppression of the neoclassical tearing mode (NTM). To determine these locations, many control systems rely on motional Stark effect constrained equilibria reconstruction and real-time Thomson scattering with TORBEAM current drive evaluation and therefore require time-intensive cross-calibration of at least two different diagnostics. Here we present a simpler, proof-of-concept analysis that uses only a single diagnostic (a radial array electron cyclotron emission radiometer) for the simultaneous determination of both the radial position of a magnetic island and the deposition location of ECCD. Measurements are compared with the modified Rutherford equation to demonstrate the effect of ECCD alignment on NTM suppression.

1. Introduction

The neoclassical tearing mode (NTM) is a metastable tearing mode that originates from a finite seed island typically on either the $m/n = 3/2$ or the $m/n = 2/1$ resonant surface (or both) and is destabilized by helical perturbations of the bootstrap current [1]. If an NTM is allowed to grow, confinement is lost across the island region. This confinement loss can lead to a decrease in plasma energy by $10-30\,\%$ in modes with $m/n = 3/2$, and, more catastrophically, to severe energy loss or disruptions in the case of a $m/n = 2/1$ mode [2]. Thus, one of the key issues for achieving stable high beta discharges in both current and future tokamaks is the control of NTMs.

An NTM can be suppressed with well-focused, high-power millimeter-wave co-current drive by replacement of the missing bootstrap current [3]. Due to its higher efficiency, scalable high power and long pulse operation, and narrow current drive at a particular harmonic resonance, radially-located electron cyclotron current drive (ECCD) is the usual choice for NTM control at DIII-D [4]. Predictably, accurate alignment of the ECCD deposition location to the resonant q-surface is essential to NTM suppression. Experimentally, alignment is usually achieved either by direct comparison of ECCD and NTM locations (such as in [5] and [6]) or by various minimum-seeking optimization algorithms (such as those described in [7].) Successful stabilization of NTMs using ECCD has been demonstrated in many tokamaks using diverse techniques, including DIII-D [4], ASDEX Upgrade [8], TEXTOR [9], Tore Supra [10], TCV [11], KSTAR [12] and JT-60U [13]. Figure 1 shows a schematic layout of ECCD/NTM alignment on a typical $m/n = 3/2$ island at DIII-D.

In DIII-D, a real-time ECCD launcher mirror control system allows for preemptive alignment of ECCD with the NTM while keeping the plasma conditions fixed, thereby maintaining a high fusion energy gain factor (e.g. $Q \sim 10$ in ITER) [14]. A standard alignment technique at DIII-D is to use motional Stark effect equilibria reconstructions (MSE-EFITs [15]) to find the NTM location and the real time TORBEAM [16] beam tracing code with a Grad-Shafranov equilibrium to determine the ECCD deposition location. However, this requires that the Grad-Shafranov solution, the q profile (for finding the location of the rational surface) and the n_e and T_e profiles (for beam tracing) are all fully correct and cross-calibrated. A system that relies on a single diagnostic and no reconstructions could be much accurate and reliable. In this paper, we extend existing techniques to show that the radial locations of both the NTM and the ECCD deposition can be simultaneously determined with a single radial array ECE diagnostic like the current DIII-D ECE system [17], eliminating the need for extensive cross-calibrations. This method is intended to be complementary to the methods developed in [14], and will allow the plasma control system to more quickly and more accurately handle NTM suppression. Furthermore, microwave diagnostics like ECE are well-suited for high-neutron environments such as ITER,

* Corresponding author.
E-mail address: ekolemen@pppl.gov (E. Kolemen).

https://doi.org/10.1016/j.fusengdes.2019.02.089
Received 6 June 2018; Received in revised form 30 December 2018; Accepted 20 February 2019
Available online 26 February 2019
0920-3796/

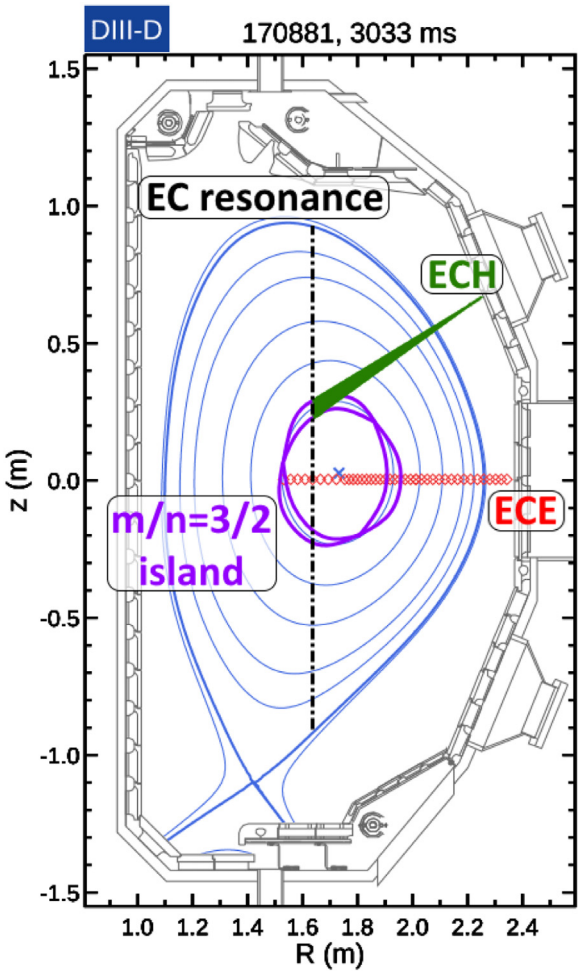

Fig. 1. Block diagram of a typical $m/n = 3/2$ suppression scenario. Note that the island width is not shown to scale and is for visualization purposes only.

since only waveguides and antennas need access to the plasma [18]. As a result, ECE will be a key component of the diagnostics suite on ITER and other future tokamaks [19].

The remainder of this paper is organized as follows. For context, in Sections 2 and 3 we briefly review the existing methods that are employed in this paper to determine the radial locations of NTMs and ECCD deposition, respectively. Then, as a proof of concept demonstration, we apply these techniques to simultaneously determine the NTM and ECCD locations for a discharge on DIII-D and compare the results with those predicted by the modified Rutherford equation in Section 4.

2. Detection of NTM location with ECE

Numerous methods to determine the radial location of magnetic islands from ECE have been developed previously. At FTU, magnetic islands are found with a phase contrast method based on the cross correlation of contiguous channels of a multichannel ECE diagnostic [20]. At JT-60U, the center of the magnetic island is detected directly from the electron temperature perturbation profile [13]. At ASDEX-U, the temperature oscillations from the magnetic island as seen by an ECE radiometer are correlated with a reference signal from one of the Mirnov coils to determine the island location [21]. At KSTAR, the alignment of the ECCD deposition with the island is estimated by X-ray imaging crystal spectroscopy [12]. At DIII-D, the matched amplitudes of island temperature fluctuations are calculated, allowing for real-time determination of the island location [5]. Importantly, other methods implemented at TEXTOR [22], TCV [23] and DIII-D [6] have included the use of oblique ECE measurements to track ECCD alignment.

In this work we follow the real-time techniques (detection of phase inversion) outlined by Park and Welander in [5] to find the location of NTMs with ECE. As a demonstration, Fig. 2 shows a calculation of the radial location of the 22 kHz NTM in DIII-D discharge 149536, in which the NTM is partially suppressed by ECCD. A typical trace of the ECE electron temperature fluctuation profile $\tilde{T}_e$ is analyzed in Fig. 2a, showing phase inversion at the NTM location. The fluctuations $\tilde{T}_e$ are convolved with a sinusoidal model of the temperature change using a matched filter to calculate the matched amplitude of $\tilde{T}_e$, as defined in [5]. Since $\tilde{T}_e$ is both phase inverted and minimized at the island center, the radial location of the island can be identified when the matched amplitude changes sign. Here we interpret linearly between signals on adjacent ECE channels to locate the NTM. In Fig. 2b the radial location of the island node found with ECE is compared to the radial location of the $q = 3/2$ surface calculated with MSE-EFITs. Smoothings of 30 ms were applied to each signal. The variations are correlated with periodic edge localized modes, which modulate the current profile in the core [5]. Note that, not only are the two calculations in good agreement, but that the ECE method obtains a higher time resolution, as is typical of ECE systems.

3. Detection of ECCD deposition location with ECE

Using the same ECE diagnostic discussed above, the ECCD deposition location can be simultaneously determined with the following procedure [24]. At DIII-D, the power (amplitude) of the ECCD launcher is modulated at 75–100 Hz. This is reflected in the ECE channels at the

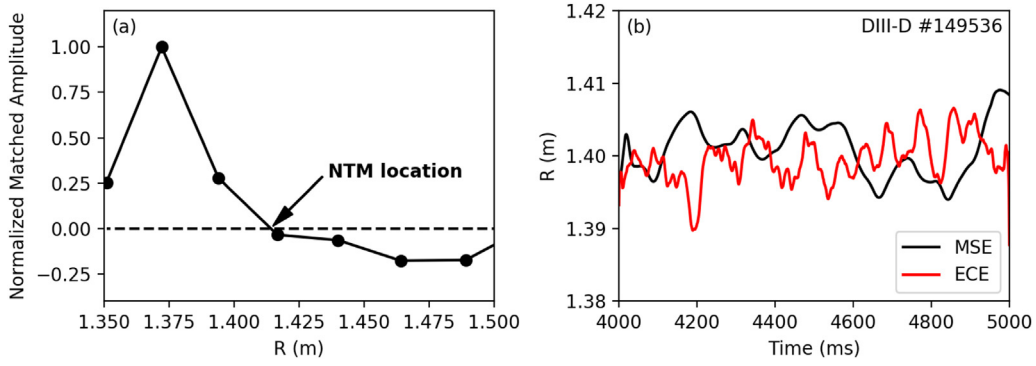

Fig. 2. DIII-D discharge 149536. (a) Normalized matched amplitude of the electron temperature fluctuation $\tilde{T}_e$ as a function of major radius at a typical time slice. The NTM location is found by linear interpolation between ECE channels when the matched amplitude switches sign. (b) The radial location R_{NTM} on the inboard midplane of a $m/n = 3/2$ magnetic island (Mirnov frequency = 22 kHz) is calculated as a function of time using MSE-EFITs ($q = m/n$) and ECE (island node from perturbed T_e) and the results are compared.

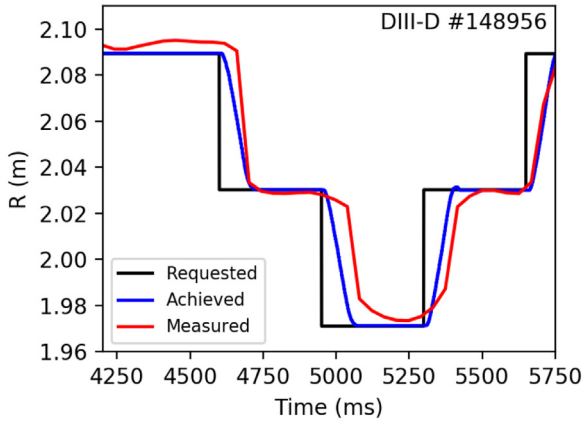

Fig. 3. DIII-D discharge 148956. Multiple step response of the mirror control; the requested and achieved positions are shown in black and blue, respectively. The ECCD deposition location as determined by ECE is displayed in red, showing good agreement with the mirror control. (For interpretation of the references to color in this figure legend, the reader is referred to the web version of this article.)

same frequency, and it is straightforward to determine the amplitude of the modulated ECCD signal present on each ECE channel. Linear interpolation is then applied to determine the peak amplitude of the modulation with respect to ECE channel number. The radial position monitored by each ECE channel depends on the magnetic field and is easily computed from MSE-EFIT. The radial location of ECCD deposition can then be found by comparing the radial locations of the ECE channels and the peak modulation amplitude.

Fig. 3 shows the ECCD deposition location for example DIII-D discharge 148956. During this discharge, the ECCD deposition location was intentionally swept over a radial range equivalent to the range viewed by five neighboring ECE channels. The main limit of this approach is the spatial resolution offered by ECE chords. For example, during DIII-D discharge 149388 (discussed below) the ECE channels are an average of ~2 cm apart (as seen in Fig. 1), limiting the spatial resolution of an ECCD measurement. For more accurate determination of the ECCD deposition location, the peak amplitude of the EC frequency modulation is interpolated between channels. Furthermore, new diagnostics at DIII-D have recently increased the possible spatial resolution of ECE measurements, further reducing the error on ECCD localization [25].

4. Using ECE for NTM suppression and control

At DIII-D, current NTM suppression techniques follow the methods described in [4,6,14]. Using real-time MSE-EFITs with advanced feedback and search algorithms, the magnetic island is targeted with steerable ECCD launcher mirrors. Island formation is detected automatically and, based on the plasma evolution and the interaction of the island and the ECCD, the ECCD alignment is adjusted. This approach requires three diagnostics (magnetics, MSE-EFIT and Thomson scattering for density) and a ray-tracing algorithm (TORBEAM), all of which must align for successful NTM control. A replacement process with a single radial ECE diagnostic requirement would reduce this cross-calibration requirement by allowing the plasma control system to independently and simultaneously locate both the ECCD deposition location and the magnetic island with a single diagnostic.

To show the feasibility of simultaneous ECE detection, the technique is applied to DIII-D discharge 149388, where the EC power was modulated at 75 Hz. Comparisons of the ECCD and NTM locations are shown in Fig. 4. In this discharge, a 26 kHz $q = 3/2$ NTM is allowed to develop after 2 s. At $t = 3.5$ s the ECCD launcher is turned on and is swept around the $q = 3/2$ resonant surface for visualization purposes. ECCD is aligned to the $q = 3/2$ magnetic island at $t = 4.25$ s and held steady for the remaining duration of the discharge, partially suppressing the NTM. As seen in Fig. 4, the ECCD deposition location and the magnetic island can now be followed throughout the duration of the shot using two different methods. In Fig. 4b, the existing TORAY-GA and MSE-EFIT codes are used to find the location of the ECCD deposition and the $n = 2$ mode, respectively. In Fig. 4c, both locations are determined simultaneously with the ECE analysis described above, without additional input from other diagnostics. The two methods show good agreement throughout the shot. Fig. 4 also highlights that even misalignments of ~1cm can significantly reduce the effectiveness of ECCD at suppressing NTMs [2], so precise alignment of the current drive is essential to effective tearing mode mitigation.

The effect of rf current drive on the NTM islands is described by the modified Rutherford equation [26]. We use the modified expression for the island width w employed in [27] and [28] to confirm NTM suppression in DIII-D discharge 149388. The island width evolves according to

$$1.\ 22^{-1}\frac{\tau_R}{r}\frac{\mathrm{dw}}{\mathrm{dt}} = \Delta' r + \epsilon^{1/2}\left(\frac{L_q}{L_p}\right)\beta_\theta\left[\frac{\mathrm{rw}}{w^2 + w_d^2} - \frac{\mathrm{rw}_{\mathrm{pol}}^2}{w^3} - \frac{8\mathrm{qr}\delta_{\mathrm{EC}}}{\pi^2 w^2}\left(\eta\frac{j_{\mathrm{EC}}}{j_{\mathrm{BS}}}\right)\right], \tag{1}$$

where the effectiveness parameter of the j_{EC} is

$$\eta = \frac{\eta_0}{1 + 2\delta_{\mathrm{EC}}^2/w^2}\exp\left[-\left(\frac{5\Delta R}{3\delta_{\mathrm{EC}}}\right)^2\right], \tag{2}$$

which accounts for the relative sizes of the island and the FWHM of the rf current drive δ_{EC}, as well as any misalignment in j_{EC}. Here τ_R is the resistive diffusion time, Δ' is assumed negative (stabilizing), $1/\epsilon = R_0/r$ is the local aspect ratio, β_θ is the poloidal beta and the coefficient η_0 is set to $\eta_0 = 0.4$ for no modulation. The q-profile and p-profile are described by $L_q \equiv q/(dq/dr) > 0$ and $L_p \equiv -p/(dp/dr) > 0$, respectively. w_d and w_{pol} are characteristic islands widths described in [26]. The FWHM of the Gaussian rf current density is given by δ_{EC}, and any misalignment of the rf current is given by ΔR. The rf current density and the bootstrap current density are given by j_{EC} and j_{BS}, respectively. Absent any coherent modulation on the mode frequency, the slow modulation of EC power requires averaging j_{EC} in Eq. (1).

The modified Rutherford equation was compared to measured island widths in DIII-D discharge 149388 to demonstrate the functionality of ECCD suppression. The island width before and after ECCD suppression can be measured with ECE by determining the size of the flattened portion of the electron temperature profile [29]. The measured width of the saturated $q = 3/2$ island before and after ECCD treatment was $w_{\mathrm{sat}} \sim 8$ cm and $w_{\mathrm{sat}} \sim 6$ cm, respectively. As shown in Fig. 5, the modified Rutherford equation accurately reproduces these values, demonstrating the validity of this approach. Here the pressure scale length L_p decreases from $L_p = 0.32$ at $w = 10$ cm to $L_p = 0.28$ at $w = 0$ cm to model the assumption that the pressure profile peaks with shrinking island size and β_θ is assumed to increase as the island shrinks from $\beta_\theta = 0.9$ to $\beta_\theta = 1$. Furthermore, $\Delta' r$ is also assumed to be a linear function of island size, increasing from $\Delta' r = -2.25$ at $w = 10$ cm to $\Delta' r = -3.85$ at $w = 0$ cm. After aligning the ECCD and the island, the averaged rf and bootstrap current densities at the island location are $j_{EC} = 130$ kA/m^2 from TORAY-GA and $j_{BS} = 180$ kA/m^2 from ONETWO respectively, so the ratio $j_{EC}/j_{BS} = 0.72$. As predicted by Eq. (1), this corresponds to a saturated island width of $w_{\mathrm{sat}} \approx 6$ cm. A ratio $j_{EC}/j_{BS} = 1.5$ is predicted to be needed for complete suppression of the NTM. Traces of the modified Rutherford equation under the plasma conditions of DIII-D discharge 149388 are seen in Fig. 5.

It should also be noted that NTM suppression as described by the modified Rutherford equation is extremely sensitive to misalignment of the rf current drive. Eq. (2) contains an $\exp[-(5\Delta R/3\delta_{EC})^2]$ term, which suggests that the ratio j_{EC}/j_{BS} needed for complete suppression increases by ~130% for a misalignment of $\Delta R/\delta_{EC} = 0.3$ in DIII-D

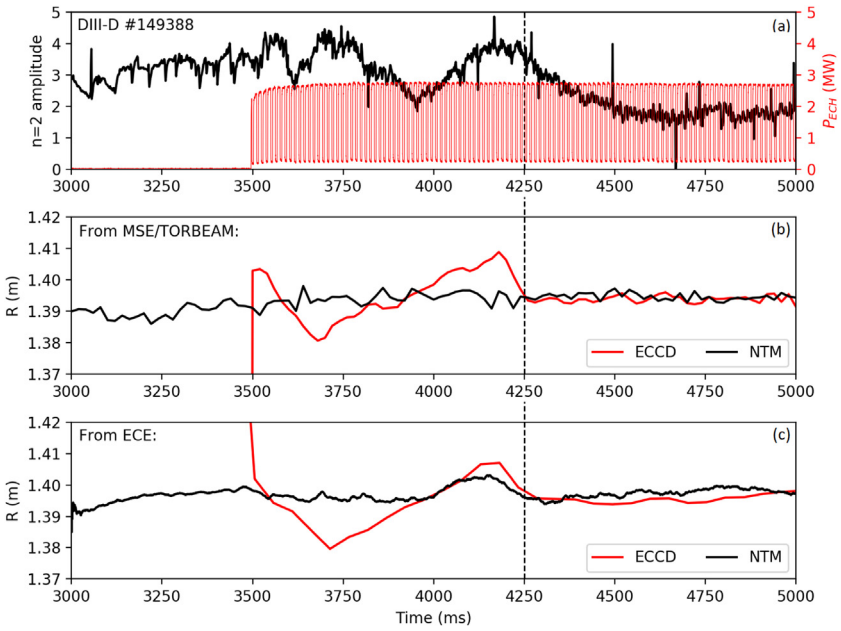

Fig. 4. DIII-D discharge 149388, where ECCD is turned on at $t = 3500$ms, swept around the island for visualization purposes, and then aligned to the NTM at $t = 4250$ ms. (Top) Amplitude of NTM perturbation ($n = 2$ mode) and ECCD power. The EC modulation frequency is 75 Hz. (Middle) Radial locations of the ECCD deposition and the NTM calculated from TORAY-GA and MSE-EFITs. (Bottom) Radial locations of the ECCD deposition and the NTM are calculated using only ECE data.

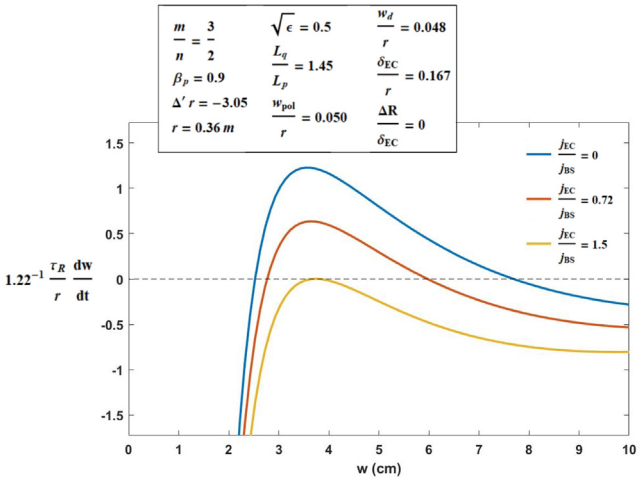

Fig. 5. Application of the modified Rutherford equation to DIII-D discharge 149388. Only the ratio j_{EC}/j_{BS} is varied, $\Delta R = 0$ is assumed.

discharge 149388. As is seen in the $n = 2$ mode amplitude signal plotted in Fig. 4, the magnetic island returns to its fully saturated value for misalignments on the order of ~ 1. This stresses the need for precise alignment of the rf current drive with the magnetic island.

5. Conclusion

In a proof of concept analysis, radial ECE is used to simultaneously locate both ECCD deposition and an NTM seed island. By comparing these measurements, NTMs could be efficiently suppressed without the time-intensive cross-calibration of various diagnostics that is needed to use MSE-EFITs and TORBEAM in a search and suppress NTM suppression scheme. Furthermore, this analysis relies only on ECE, which is ticked to be a main diagnostic on ITER since it is well-suited for high neutron environments. Comparisons with the modified Rutherford equation highlight the effectiveness of ECCD at suppressing NTMs, but also stress the need for accurate alignment with the seed island. Future work includes the real-time application of this scheme to plasma discharges in DIII-D as a method of efficient NTM avoidance.

Disclaimer

Acknowledgments

This research was supported in part by the United States Department of Energy (DoE) under contract numbers DC-AC02-09Ch11466, DE-AC52-07NA27344, DE-FC02-04ER54698, ED-AC05-00OR22725 and DE-FOA-0001386: Early Career Research Program.

References

[1] Z. Chang, J. Callen, E. Fredrickson, R. Budny, C. Hegna, K. Mcguire, M. Zarnstorff, the TFTR Group, Observation of nonlinear neoclassical pressure-gradient driven tearing modes in TFTR, Phys. Rev. Lett. 74 (23) (1995), https://doi.org/10.1103/PhysRevLett.74.4663.

[2] R. Prater, R. La Haye, T.T. Luce, C.C. Petty, E.E. Strait, J.J. Ferron, D.D. Humphreys, A. Isayama, J. Lohr, K. Nagasaki, P.P. Politzer, M.M. Wade, A.A. Welander, R.L. Haye, T.T. Luce, C.C. Petty, E.E. Strait, J.J. Ferron, D.D. Humphreys, A. Isayama, J. Lohr, K. Nagasaki, P.P. Politzer, M.M. Wade, A.A. Welander, Stabilization and prevention of the 2/1 neoclassical tearing mode for improved performance in DIII-D, Nucl. Fusion 47 (2007) 371, https://doi.org/10.1088/0029-5515/47/5/001 http://stacks.iop.org/0029-5515/47/i=5/a=001?key=crossref.846087b944145f23d54ce507eaba8e6a.

[3] R. Prater, Heating and current drive by electron cyclotron waves, Phys. Plasmas 11 (2004) 2349, https://doi.org/10.1063/1.1690762.

[4] R.J. La Haye, Neoclassical tearing modes and their control, Phys. Plasmas 13 (2006) 055501, https://doi.org/10.1063/1.1694232.

[5] Y.S. Park, A.S. Welander, Real-time determination of magnetic island location for neoclassical tearing mode control in DIII-D, Plasma Phys. Control. Fusion 48 (2006) 1447, https://doi.org/10.1088/0741-3335/48/9/013.

[6] F.A.G. Volpe, M.E. Austin, R.J. La Haye, J. Lohr, R. Prater, E.J. Strait, A.S. Welander, Advanced techniques for neoclassical tearing mode control in DIII-

D, Phys. Plasmas 16 (2009) 102502, https://doi.org/10.1063/1.3232325.
[7] W. Wehner, E. Schuster, Control-oriented modelling for neoclassical tearing mode stabilization via minimum-seeking techniques, Nucl. Fusion 52 (2012) 074003, https://doi.org/10.1088/0029-5515/52/7/074003.
[8] M. Maraschek, G. Gantenbein, Q. Yu, H. Zohm, S. Günter, F. Leuterer, A. Manini, F. Leuterer, A. Manini, Enhancement of the stabilization efficiency of a neoclassical magnetic island by modulated electron cyclotron current drive in the ASDEX upgrade tokamak, Phys. Rev. Lett. 98 (2007) 025005, https://doi.org/10.1103/PhysRevLett.98.025005.
[9] B.A. Hennen, E. Westerhof, P.W.J.M. Nuij, J.W. Oosterbeek, M.R. de Baar, W.A. Bongers, A. Bürger, D.J. Thoen, M. Steinbuch, t.T. Team, Real-time control of tearing modes using a line-of-sight electron cyclotron emission diagnostic, Plasma Phys. Control. Fusion 52 (2010) 104006, https://doi.org/10.1088/0741-3335/52/10/104006.
[10] M. Lennholm, G. Agarici, G. Berger-By, P. Bosia, F. Bouquey, E. Cellier, J. Clary, M. Clapit, C. Darbos, G. Giruzzi, M. Jung, R. Magne, D. Roux, J.L. Segui, E. Traisnel, X. Zou, The ECRH/ECCD system on Tore Supra, a major step towards continuous operation, Nucl. Fusion 43 (2003) 1458, https://doi.org/10.1088/0029-5515/43/11/019 http://stacks.iop.org/0029-5515/43/i=11/a=019?key=crossref.c0bfaadfd599f28cb43b922e00c1e900.
[11] F. Felici, T.P. Goodman, O. Sauter, G. Canal, S. Coda, B.P. Duval, J.X. Rossel, the TCV Team, Integrated real-time control of MHD instabilities using multi-beam ECRH/ECCD systems on TCV, Nucl. Fusion 52 (2012) 74001, https://doi.org/10.1088/0029-5515/52/7/074001.
[12] K. Kim, Y.S. Na, M. Kim, Y.M. Jeon, K.D. Lee, J.G. Bak, M.J. Choi, G.S. Yun, S.G. Lee, S. Park, J.H. Jeong, L. Terzolo, D.H. Na, M.G. Yoo, Team t.K, Experiment and simulation of tearing mode evolution with electron cyclotron current drive in KSTAR, Curr. Appl. Phys. 15 (2015) 547–554, https://doi.org/10.1016/J.CAP.2015.01.032 https://www.sciencedirect.com/science/article/pii/S1567173915000413.
[13] A. Isayama, Y. Kamada, N. Hayashi, T. Suzuki, T. Oikawa, T. Fujita, T. Fukuda, S. Ide, H. Takenaga, K. Ushigusa, T. Ozeki, Y. Ikeda, N. Umeda, H. Yamada, M. Isobe, Y. Narushima, K. Ikeda, S. Sakakibara, K. Yamazaki, K. Nagasaki, the JT-60 Team, Achievement of high fusion triple product, steady-state sustainment and real-time NTM stabilization in high-p ELMy H-mode discharges in JT-60U, Nucl. Fusion 43 (2003) 1272–1278, https://doi.org/10.1088/0029-5515/43/10/031 http://stacks.iop.org/0029-5515/43/i=10/a=031?key=crossref.2b523dc4fd54c452b334a78b5c9d770e.
[14] E. Kolemen, A.S. Welander, R.J. La Haye, N.W. Eidietis, D.A. Humphreys, J. Lohr, V. Noraky, B.G. Penaflor, R. Prater, F. Turco, State-of-the-art neoclassical tearing mode control in DIII-D using real-time steerable electron cyclotron current drive launchers, Nucl. Fusion 54 (2014) 073020, https://doi.org/10.1088/0029-5515/54/7/073020 http://stacks.iop.org/0029-5515/54/i=7/a=073020?key=crossref.e5c1ab404443aedbbd06b2a15441021d.
[15] C.T. Holcomb, M.A. Makowski, S.L. Allen, W.H. Meyer, M.A. Van Zeeland, Overview of equilibrium reconstruction on DIII-D using new measurements from an expanded motional Stark effect diagnostic, Rev. Sci. Instrum. 79 (2008) 10F518, https://doi.org/10.1063/1.2955711.
[16] E. Poli, A.G. Peeters, G.V. Pereverzev, TORBEAM, a beam tracing code for electron-cyclotron waves in tokamak plasmas, Comput. Phys. Commun. 136 (2001) 90–104, https://doi.org/10.1016/S0010-4655(01)00146-1 https://www.sciencedirect.com/science/article/pii/S0010465501001461.
[17] M.E. Austin, J. Lohr, Electron cyclotron emission radiometer upgrade on the DIII-D tokamak, Rev. Sci. Instrum. 74 (2003) 1457, https://doi.org/10.1063/1.1530387.
[18] A.E. Costley, T. Sugie, G. Vayakis, C.I. Walker, Technological challenges of ITER diagnostics, Fusion Eng. Des. 74 (2005) 109–119, https://doi.org/10.1016/j.fusengdes.2005.08.026 https://ac.els-cdn.com/S092037960500390X/1-s2.0-S092037960500390X-main.pdf?_tid=bfaccc96-4cc1-4f34-8e0a-3f9b3c7db7bc&acdnat=1521049802_6b27281f076373529930f096cdbefe94.
[19] H.K.B. Pandya, R. Kumar, S. Danani, P. Shrishail, S. Thomas, V. Kumar, G. Taylor, A. Khodak, W.L. Rowan, S. Houshmandyar, V.S. Udintsev, N. Casal, M.J. Walsh, ITER ECE diagnostic: design progress of IN-DA and the diagnostic role for physics, J. Phys.: Conf. Ser. 823 (2017) 012033, https://doi.org/10.1088/1742-6596/755/1/011001.
[20] J. Berrino, E. Lazzaro, S. Cirant, G. D'Antona, F. Gandini, E. Minardi, G. Granucci, Electron cyclotron emission temperature fluctuations associated with magnetic islands and real-time identification and control system, Nucl. Fusion 45 (2005) 1350, https://doi.org/10.1088/0029-5515/45/11/016.
[21] A. Keller, F. Leuterer, M. Maraschek, W. Suttrop, H. Zohm, t. A. U. Team, Analysis methods and conditions for feedback controlled NTM stabilization, 30th EPS Conference on Contr. Fusion and Plasma Physics 27A (2003) P-1.130, http://citeseerx.ist.psu.edu/viewdoc/download?. doi=10.1.1.944.8781&rep=rep1&type=pdf http://epsppd.epfl.ch/StPetersburg/PDF/P1_130.PDF.
[22] W.A. Bongers, A.P.H. Goede, E. Westerhof, J.W. Oosterbeek, N.J. Doelman, F.C. Schüller, M.R. de Baar, W. Kasparek, W. Wubie, D. Wagner, J. Stober, t.T. Team, Magnetic island localization for NTM control by ECE viewed along the same optical path of the ECCD beam, Fusion Sci. Technol. 55 (2008) 1536, https://doi.org/10.13182/FST09-A4071.
[23] U.A. Sheikh, B.P. Duval, C. Galperti, M. Maraschek, O. Sauter, C. Sozzi, G. Granucci, M. Kong, B. Labit, A. Merle, N. Rispoli, T.T.C.V. Team, T.E.M. Team, Disruption avoidance through the prevention of NTM destabilization in TCV, Nucl. Fusion 58 (2018) 106026, https://doi.org/10.1088/1741-4326/aad924 http://stacks.iop.org/0029-5515/58/i=10/a=106026.
[24] R. Prater, R.J. La Haye, J. Lohr, T.C. Luce, C.C. Petty, J.R. Ferron, D.A. Humphreys, E.J. Strait, F.W. Perkins, R.W. Harvey, Discharge improvement through control of neoclassical tearing modes by localized ECCD in DIII-D, Nucl. Fusion 43 (2003) 1128, https://doi.org/10.1088/0029-5515/43/10/014/pdf.
[25] C. Sung, W.A. Peebles, C. Wannberg, T.L. Rhodes, X. Nguyen, R. Lantsov, L. Bardóczi, A frequency tunable, eight-channel correlation ECE system for electron temperature turbulence measurements on the DIII-D tokamak, Rev. Sci. Instrum. 87 (2016) 11E123, https://doi.org/10.1063/1.4961296.
[26] R. La Haye, R. Buttery, S. Guenter, G. Huysmans, M. Maraschek, H. Wilson, Dimensionless scaling of the critical beta for onset of a neoclassical tearing mode, Phys. Plasmas 7 (2000) 3349, https://doi.org/10.1063/1.872487.
[27] R.J. La Haye, S. Günter, D.A. Humphreys, J. Lohr, T.C. Luce, M.E. Maraschek, C.C. Petty, R. Prater, J.T. Scoville, E.J. Strait, Control of neoclassical tearing modes in DIIID, Phys. Plasmas 9 (2002) 2051, https://doi.org/10.1063/1.1456066.
[28] C.C. Petty, R.J. La Haye, T.C. Luce, D.A. Humphreys, A.W. Hyatt, J. Lohr, R. Prater, E.J. Strait, M.R. Wade, Complete suppression of the m = 2/n = 1 neoclassical tearing mode using electron cyclotron current drive in DIII-D, Nucl. Fusion 44 (2004) 243, https://doi.org/10.1088/0029-5515/44/2/004 http://stacks.iop.org/0029-5515/44/i=2/a=004?key=crossref.9c330772ec958b9059de390dc6e2a480.
[29] Z. Chang, E.D. Fredrickson, S.H. Batha, M.G. Bell, R.V. Budny, F.M. Levinton, K.M. Mcguire, G. Taylor, M.C. Zarnstorff, T. Group, the TFTR Group, Neoclassical tearing modes in Tokamak Fusion Test Reactor experiments. I. Measurements of magnetic islands and, Phys. Plasmas 5 (1998) 1076, https://doi.org/10.1063/1.872627.